Supporting Information

N-to-S Substitution Induced Fluorescence-to-Phosphorescence Dominant Emission with Excitation-Dependent Intersystem Crossing

Guoyan Li, Yexin Li, Xiaofeng Yang, Jinling Miao, Yu Cui, Yong Nie, Shuaijun Yang, Wei Liu, and Guoxin Sun**

Materials and Instrumentation. All chemicals including dry tetrahydrofuran and DMF were obtained from Energy Chemical, ^{1}H and ^{13}C NMR spectra were measured on a Bruker Avance 400/600 MHz spectrometer. High-resolution mass spectra (HRMS) were carried out on a Shimadzu LCMS-IT-TOF mass spectrometer at an APCI mode using CH_2Cl_2 as solvent. High performance liquid chromatography (HPLC) analysis was conducted on a Shimadzu LC-20AT system. Absorption spectra in solution were performed on a Persee TU-1901 spectrophotometer. Solid-state absorption was recorded on a Shimadzu UV-3600 Plus spectrophotometer in diffuse reflectance mode. Photoluminesscence spectrum, absolute quantum yield, and lifetime were all recorded on an Edinburgh Instruments FLS920/1000. X-ray powder diffraction patterns were recorded on a Bruker D8 Focus diffractometer equipped with Cu Kα radiation. The electron paramagnetic resonance (EPR) spectroscopy was performed on a Bruker A300 instrument.

Single-crystal X-ray diffraction measurements were performed on an Agilent Xcalibur, Eos, Gemini or Bruker D8 Venture diffractometer. The structures were solved by the direct methods and refined by a full-matrix least squares technique on F^2 using SHELXL programs.[1,2] CCDC 2209689 (BECA), 2216485 (BDTA-a), and 2216489 (BDTA-b) contain the supplementary crystallographic data. These data can be obtained free of charge from the Cambridge Crystallographic Data Centre via www.ccdc.cam.ac.uk/data_request/cif.

Computational detail. For the solid-state calculation, the geometries of interacting dimer were directly extracted from the crystal structure without further optimization. TD-DFT was used to calculate the electronic transition energies from S_0 to S_n and T_n states at CAM-B3LYP/def2-TZVP level, which was performed on Gaussian 09 software.[3] The hole-electron analysis was performed on Multiwfn.[4,5] The SOC constants were calculated on Orca 5 at CAM-B3LYP/ZORA-def2-TZVP level.[6]

Synthesis. 6-Bromo-*N*-ethylcarbazole-3-carboxaldehyde (BECA). A solution of *N*-bromosuccinimide (2.72 g, 15.28 mmol) in *N,N*-dimethylformamide (25 mL) was added dropwise into a solution of *N*-ethylcarbazole carboxaldehyde (3.10 g, 13.90 mmol) in *N,N*-dimethylformamide (25 mL) at 0°C. After stiring for 1 hour. 20 mL of saturated brine was added. Then the mixture was extracted with dichloromethane (50×3 mL). The organic phases were combined, and the solvent was removed by a rotary evaporator. The crude product was purified by column chromatography (petroleum ether:ethyl acetate = 8:1) to yield a white powder (2.26 g, 53.8%). ^{1}H NMR (400 MHz, $CDCl_3$) δ: 10.10 (s, 1H) , 8.56 (s, 1H), 8.28 (d, J = 2.0 Hz, 1H), 8.05 (dd, J = 8.4, 1.2 Hz, 1H), 7.62 (dd, J = 8.4, 2.0 Hz, 1H), 7.49 (d, J = 8.4 Hz, 1H), 7.35 (d, J = 8.4 Hz, 1H), 4.40 (q, J = 7.2 Hz, 2H), 1.47 (t, J = 7.2 Hz, 3H). ^{13}C NMR (151 MHz, $CDCl_3$) δ: 191.70, 143.86, 139.45, 129.58, 129.03, 127.67, 124.91, 124.57, 123.72, 122.22, 113.32, 110.73, 109.18, 38.26, 13.93. APCI-HRMS (m/z) calcd for $C_{15}H_{13}BrNO$ $[M+H]^+$: 302.0175; found: 302.0171.

8-Bromodibenzothiophene-2-carboxaldehyde (BDTA). Under argon atmosphere, n-BuLi (2.5 M, 3.5 mL, 8.75 mmol) was added dropwise to a solution of 2,8-dibromodibenzothiophene (3.0 g, 8.77 mmol) in tetrahydrofuran (80 mL) at -75°C with stirring. The turbid liquid turns yellow immediately. After stirring at -75 °C for 1 h, dry *N,N*-dimethylformamide (0.7 mL, 9.08 mmol) was added slowly. The color changes from yellow to light brown. After another 1 h, the reaction mixture was allowed to warm to room temperature and stirred overnight. Then saturated $NaHCO_3$ solution (150 mL) was added to the mixture. After filtration, the filtrate was extracted three times with dichloromethane (50 × 3 mL). The organic phases were combined, and the solvent was removed by a rotary evaporator. Then he crude solid was purified by column chromatography (petroleum ether/dichloromethane = 12:1)

to yield a white powder (0.527 g, 20.7%). ^{1}H NMR (400 MHz, $CDCl_3$) δ: 10.16 (s, 1H), 8.60 (s, 1H), 8.39 (d, J = 2.0 Hz, 1H), 8.00 (s, 2H), 7.76 (d, J = 8.4 Hz, 1H), 7.63 (dd, J = 8.4, 2.0 Hz, 1H). ^{13}C NMR (151 MHz, $CDCl_3$) δ: 192.00, 191.64, 146.60, 138.47, 136.83, 135.01, 133.58, 130.77, 127.53, 125.12, 124.44, 124.01, 123.63, 119.29. APCI-HRMS (m/z) calcd for $C_{13}H_8BrOS$ $[M+H]^+$: 290.9474; found: 290.9481.

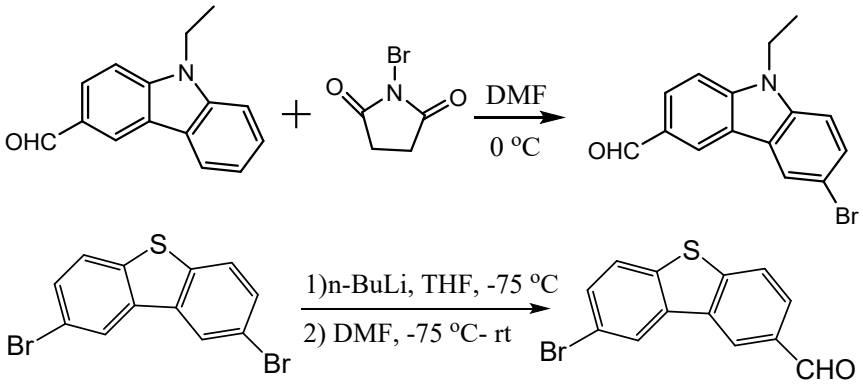

Scheme S1. Synthetic routes.

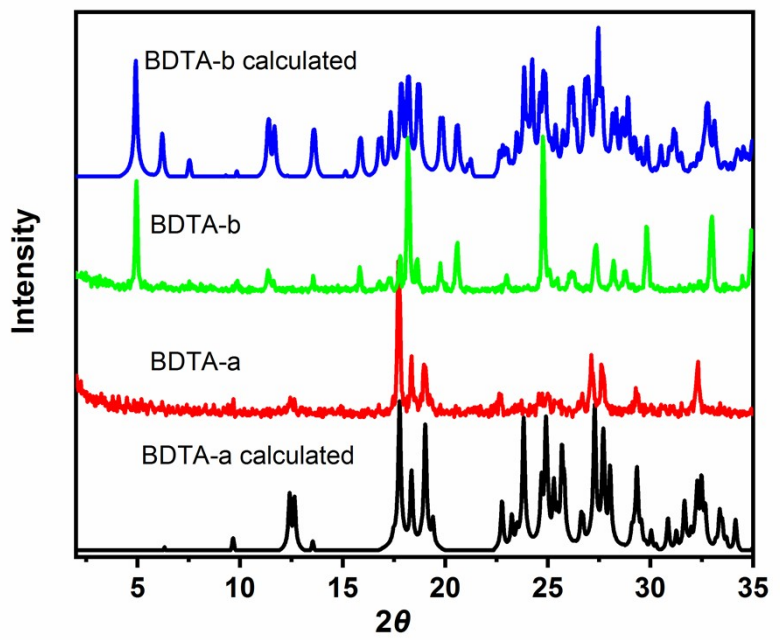

Figure S1. The XRD patterns of BDTA polymorphs. For comparison, the calculated XRD diffractograms from crystal structures are also provided.

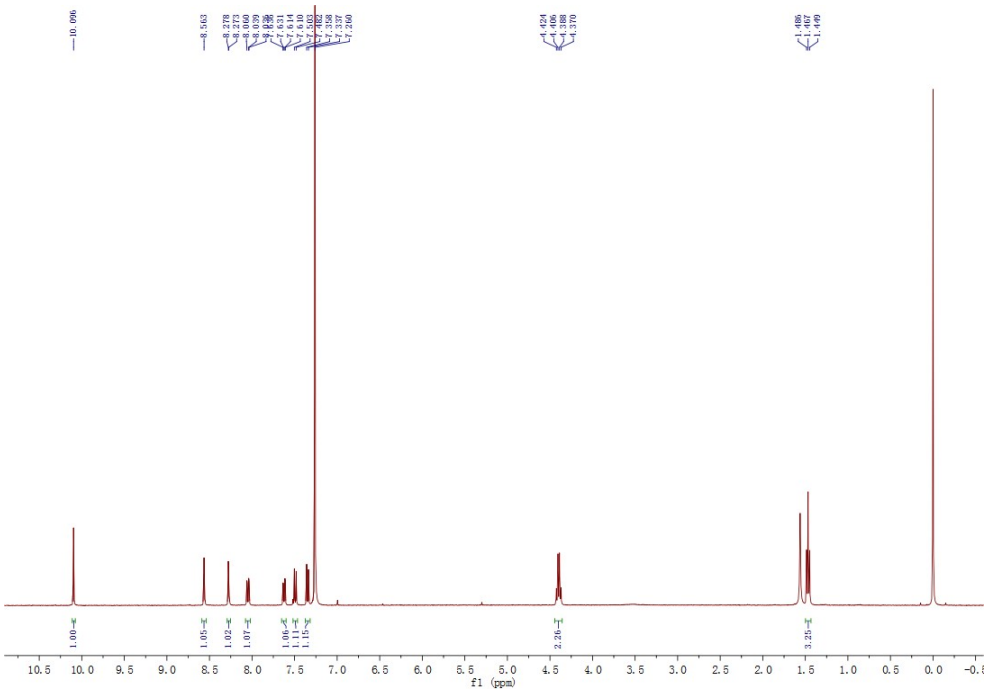

Figure S2. ^{1}H NMR spectrum of BECA in $CDCl_3$ solution.

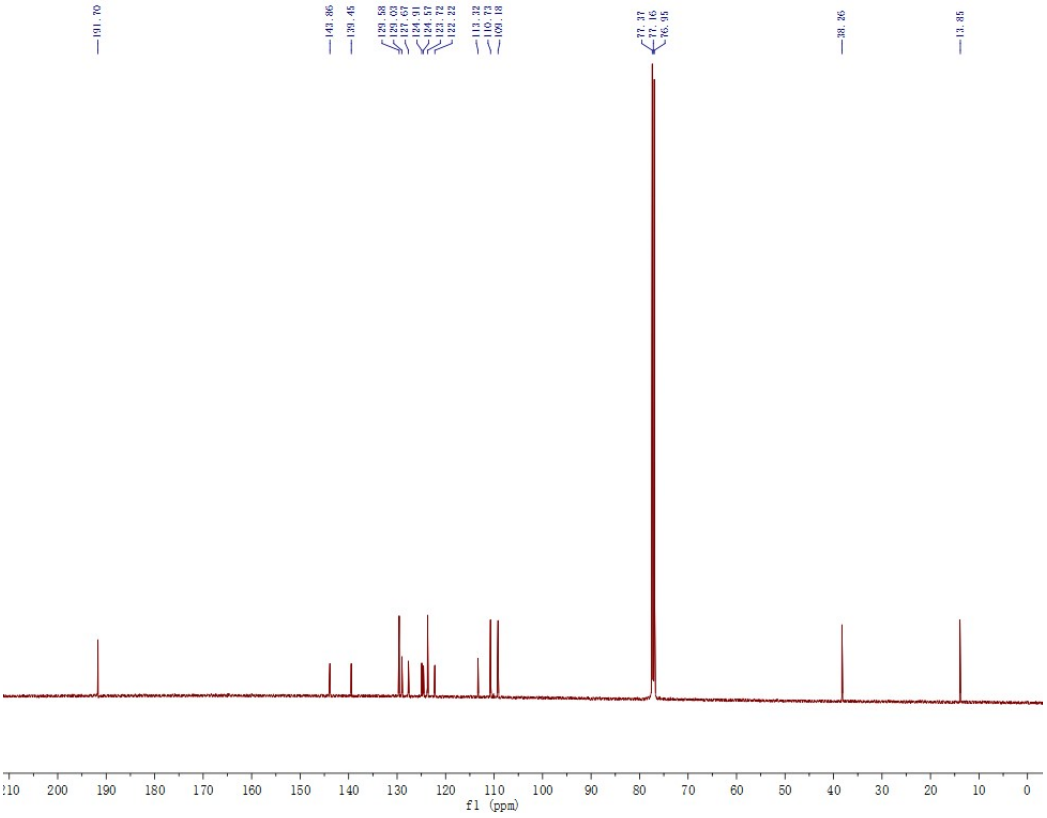

Figure S3. ^{13}C NMR spectrum of BECA in $CDCl_3$ solution.

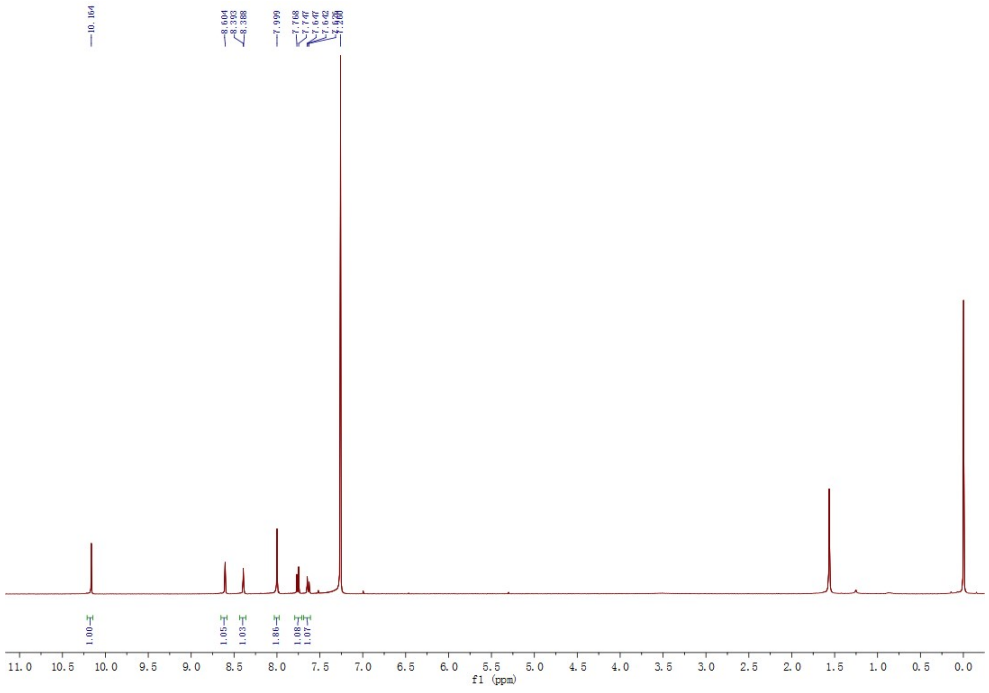

Figure S4. ^{1}H NMR spectrum of BDTA in $CDCl_3$ solution.

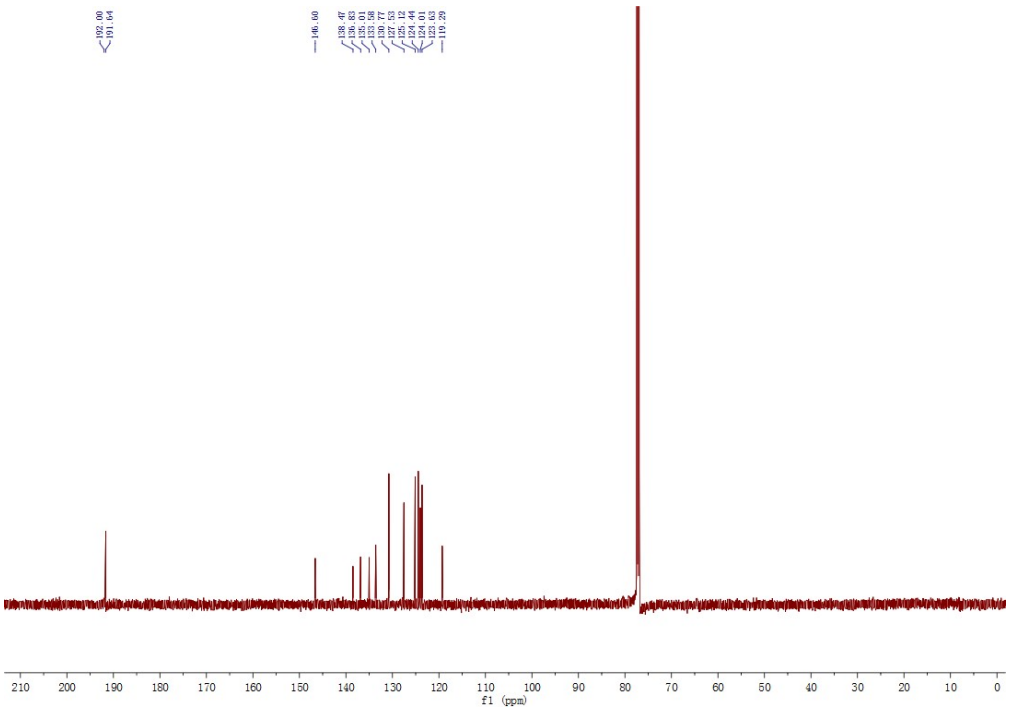

Figure S5. ^{13}C NMR spectrum of BDTA in $CDCl_3$ solution.

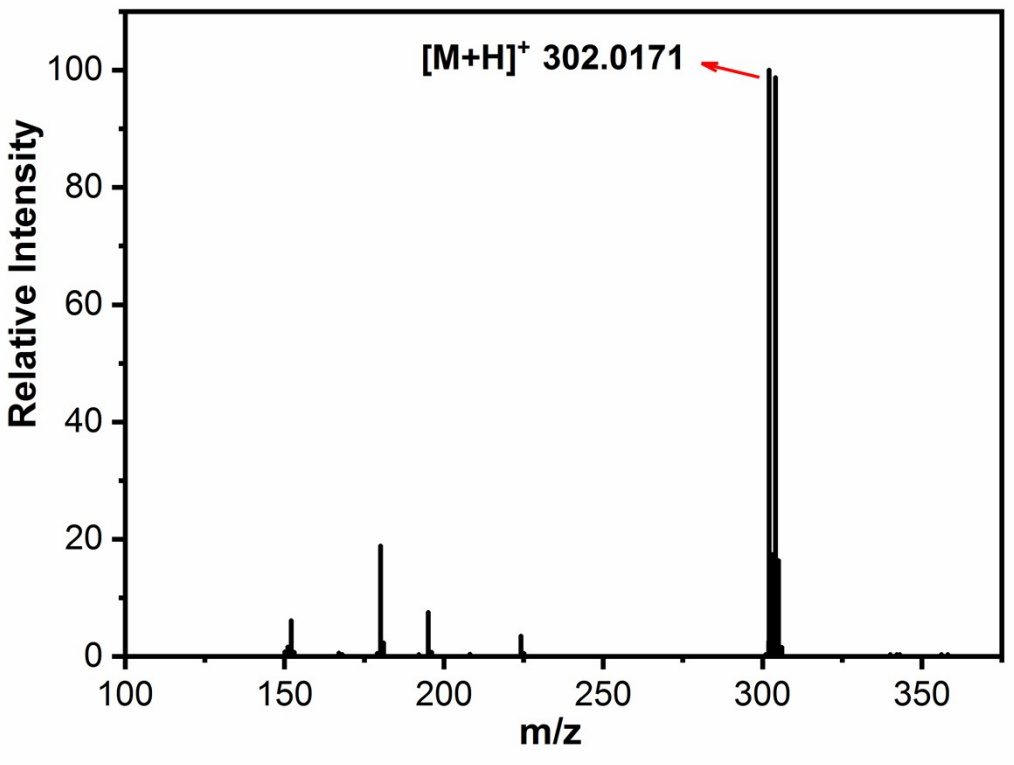

Figure S6. HR-MS spectrum of BECA.

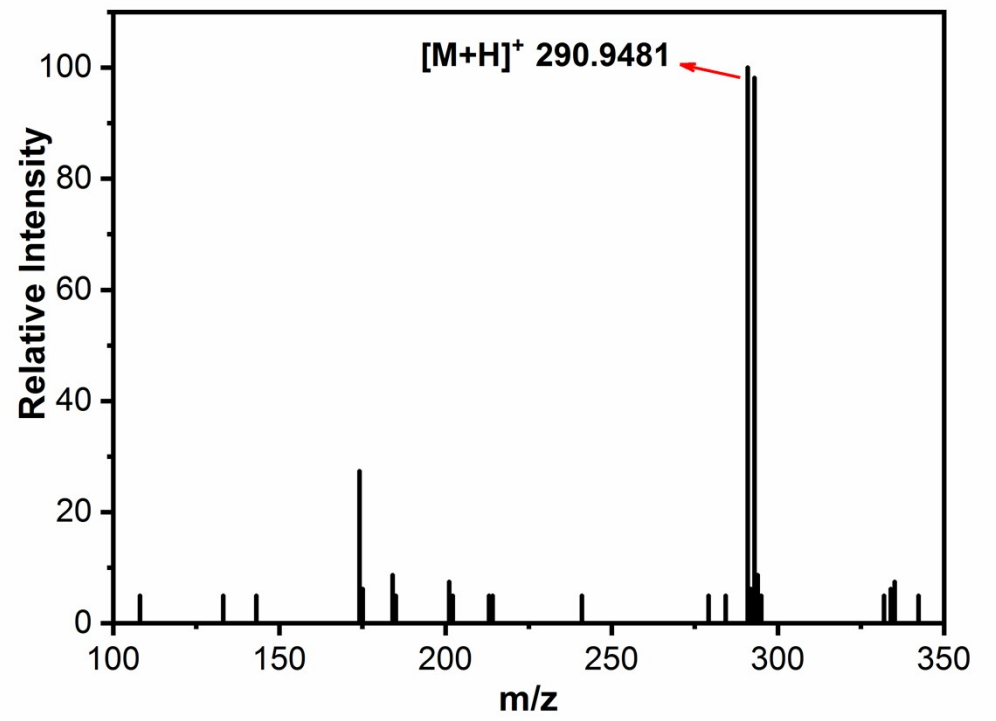

Figure S7. HR-MS spectrum of BDTA.

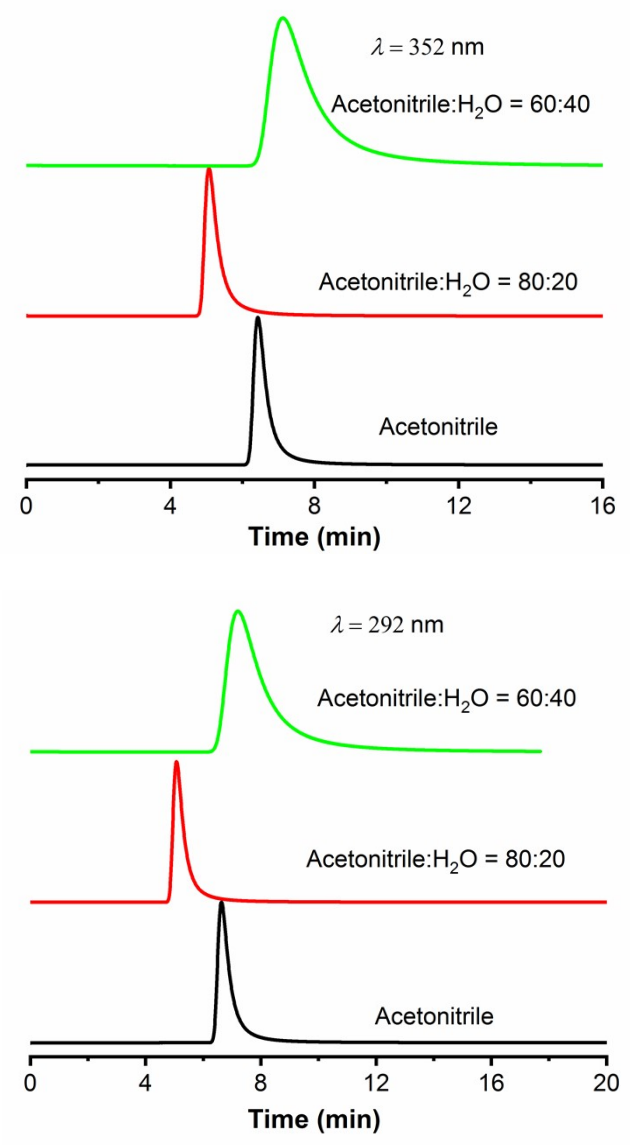

Figure S8. HPLC curves of BECA in pure acetonitrile and acetonitrile/H_2O mixture in the ratios of 80:20 and 60:40 by monitoring at 352 and 292 nm, respectively.

As is proved that the trace of isomeric impurity (1H-benzo[*f*]indole) in commercial carbazole plays an important role in the RTP property of carbazole derivatives. Herein, the purity of BECA was cautiously detected. As shown in Figure S8, the HPLC tests were monitored at two wavelengths (292 and 352 nm), and both pure acetonitrile and acetonitrile/H_2O mixture with different ratio were used as eluent. The results show that the BECA product is in high purity.

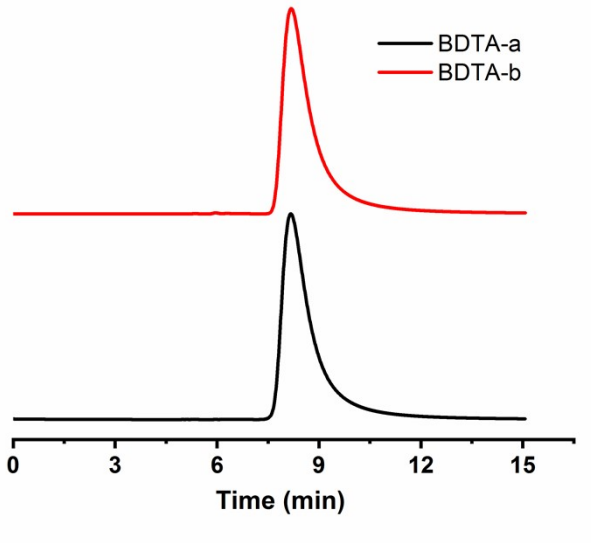

Figure S9. HPLC curves of two BDTA polymorphs in pure acetonitrile by monitoring at 292 nm.

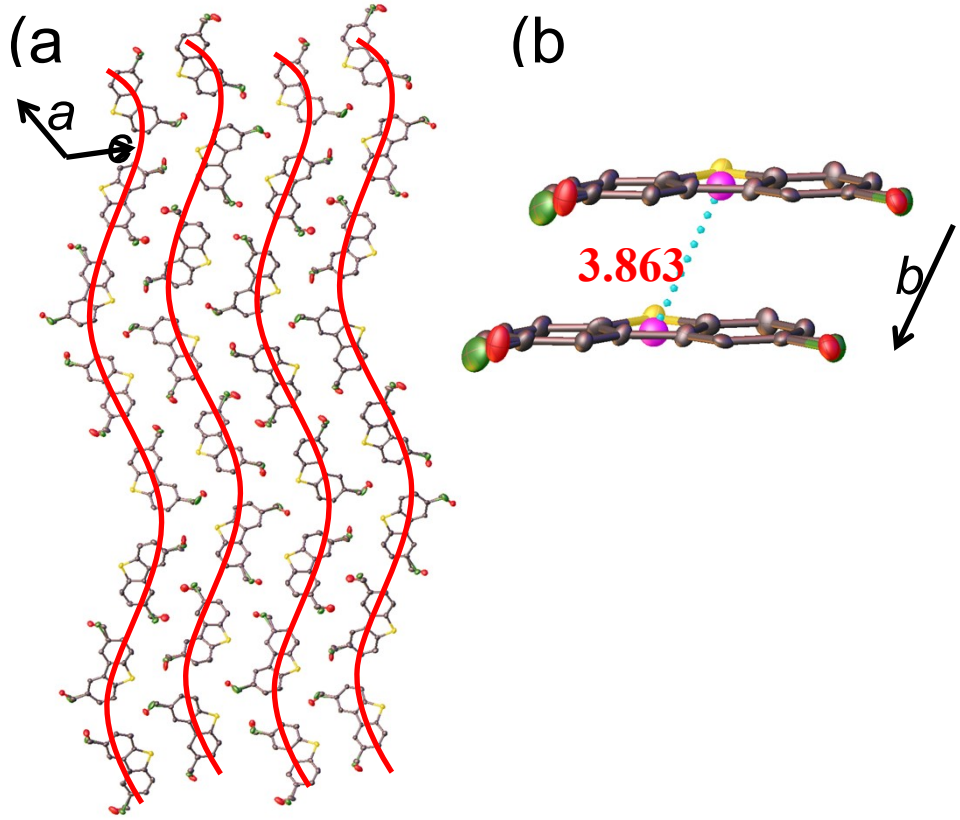

Figure S10. (a) The crystal packing of BDTA-b in the *ac* plane. (b) The centroid···centroid distance between adjacent molecules along the *b* axis. Hydrogen atoms are omitted for clarity.

Table S1. X-ray crystal structural data.

	BECA	BDTA-a	BDTA-b
Chemical formula	$C_{15}H_{12}BrNO$	$C_{13}H_7BrOS$	$C_{13}H_7BrOS$
Formula Mass	302.17	291.16	291.16
Crystal system	orthorhombic	monoclinic	monoclinic
Space group	$P2_12_12_1$	C2/c	*P*2/c
a/Å	4.3021(2)	28.9708(13)	39.011(3)
b/Å	11.0405(6)	3.86710(10)	3.8629(2)
c/Å	26.4287(15)	20.0178(9)	30.980(2)
α/°	90	90	90
β/°	90	105.170(2)	113.013(2)
γ/°	90	90	90
V/Å^3	1255.29(11)	2164.50(15)	4297.0(5)
Temperature/K	170	170	170
Z	4	8	16
Density/Mg/m^3	1.599	1.787	1.800
No. of reflections measured	19728	14057	7619
No. of independent reflections	2204	1869	7619
R_{int}	0.0862	0.0347	-
R_1 ($I > 2\sigma(I)$)	0.0938	0.0876	0.1135
wR_2 ($I > 2\sigma(I)$)	0.2215	0.3244	0.2496
R_1 (all data)	0.0964	0.0910	0.1217
wR_2 (all data)	0.2227	0.3333	0.2531
Goodness of fit on F^2	1.215	1.092	1.219

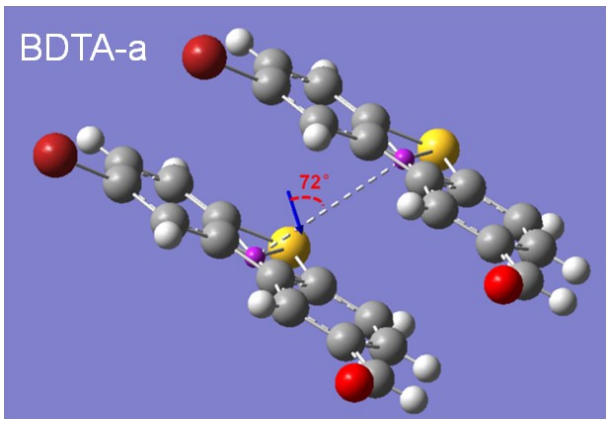

Figure S11. The angle between line of molecule center and the direction (blue arrow) of transition dipole. The dimer was extracted from the BDTA-a crystal structure.

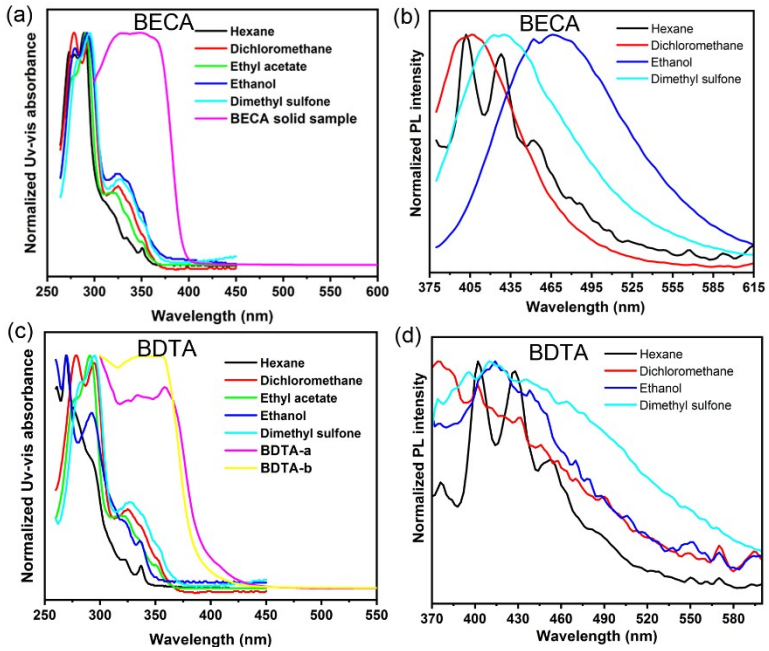

Figure S12. The absorption (a) (c) and emission (b) (d) spectra of BECA and BDTA in solution at room temperature. For comparison, the solid-state absorption is also present.

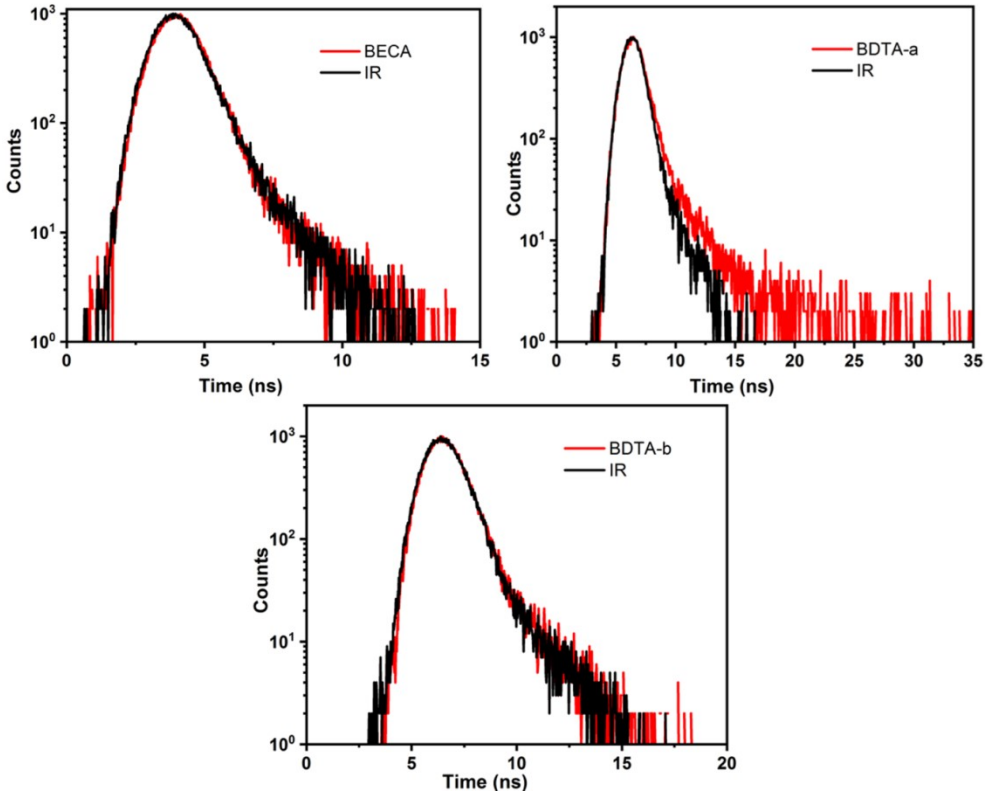

Figure S13. The solid-state fluorescence decay curves monitored at 405 nm for BECA and 420 nm for BDTA polymorphs.

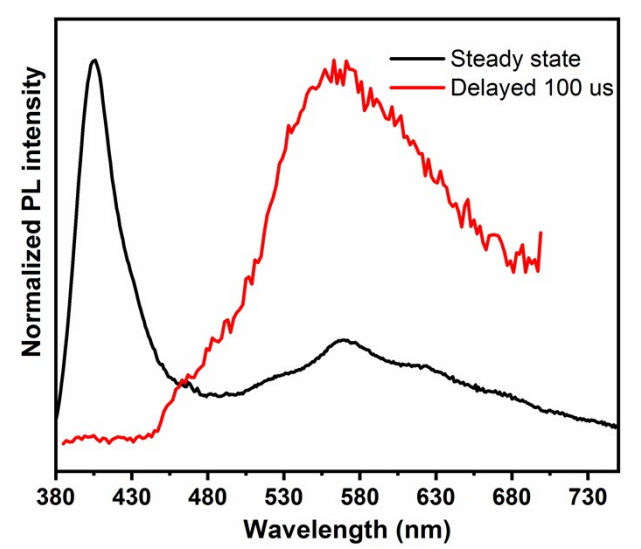

Figure S14. The steady-state and delayed emission spectra of BECA solid at room temperature (λ_{ex} = 340 nm).

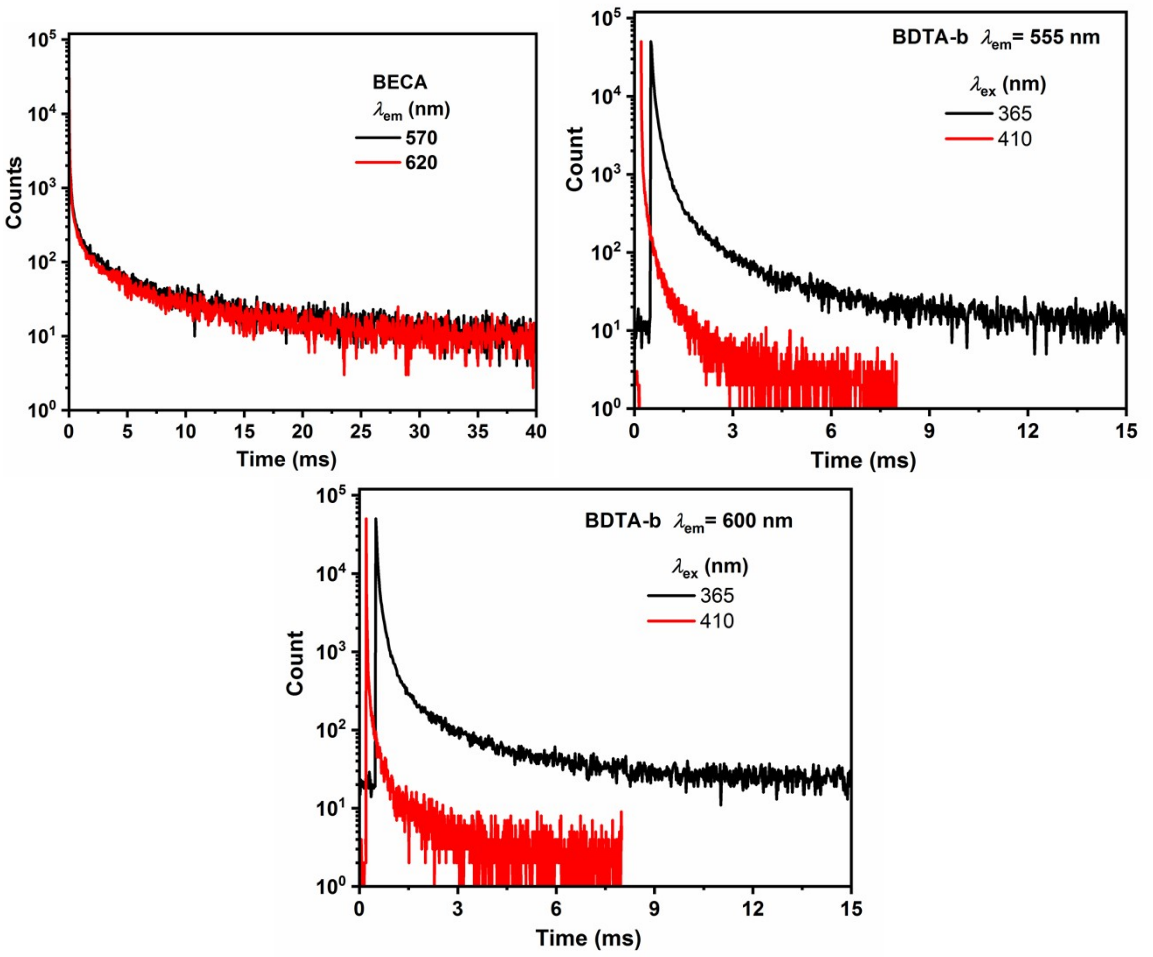

Figure S15. The phosphorescence decay curves.

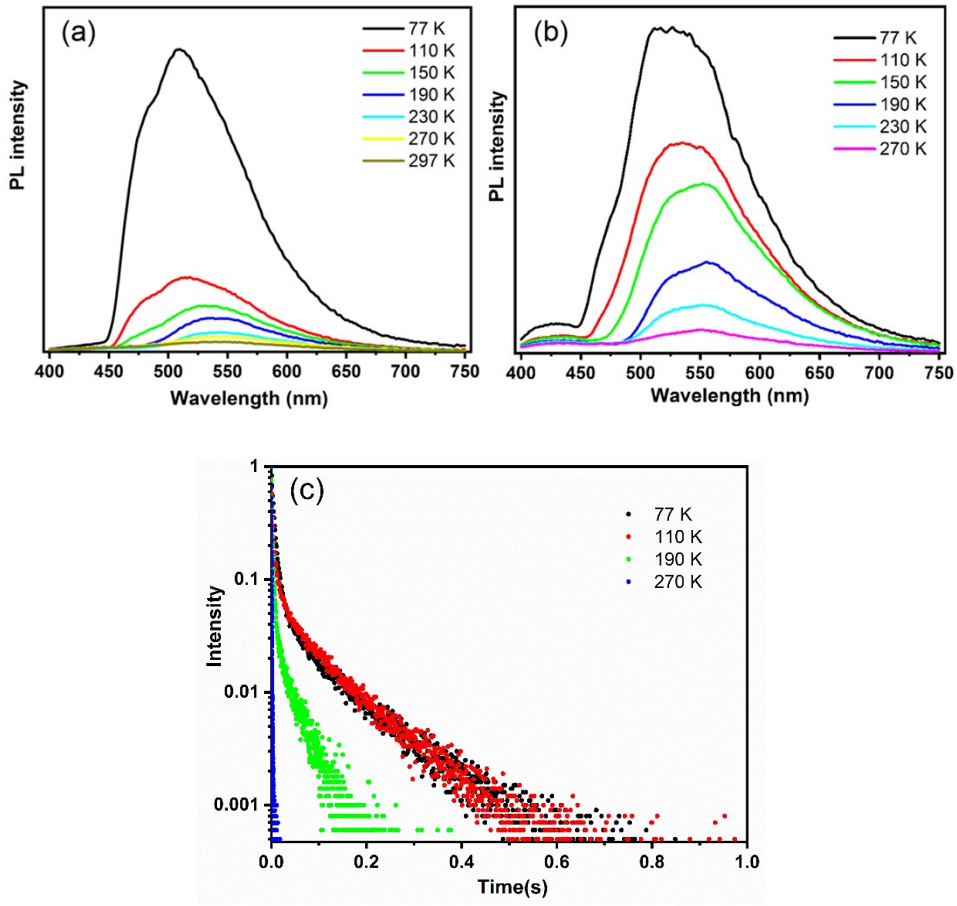

Figure S16. The change of PL spectrum of BDTA-a (a) and BDTA-b (b) with temperature. λ_{ex} = 380 nm. (c) The transient luminescence decay spectra of BDTA-b at different temperature.

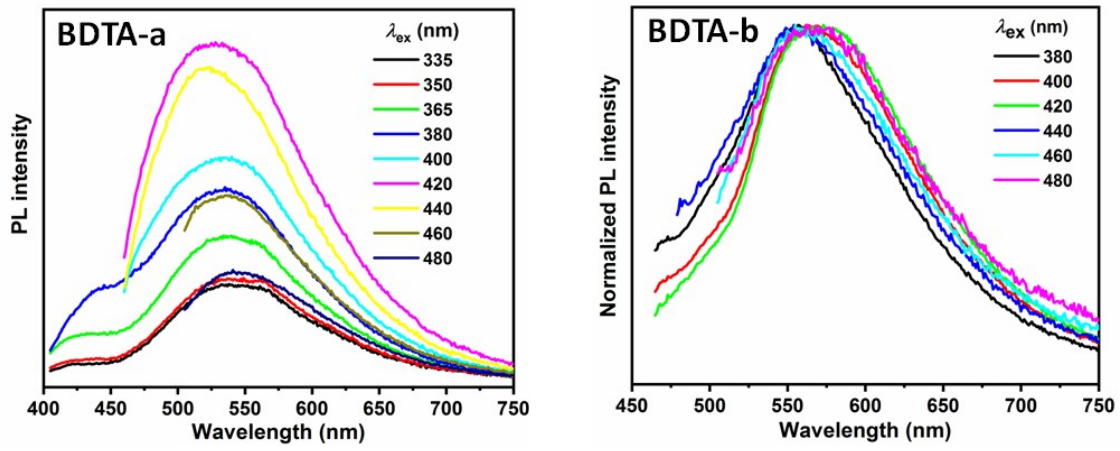

Figure S17. The emission spectra of BDTA-a and BDTA-b upon different excitation wavelengths.

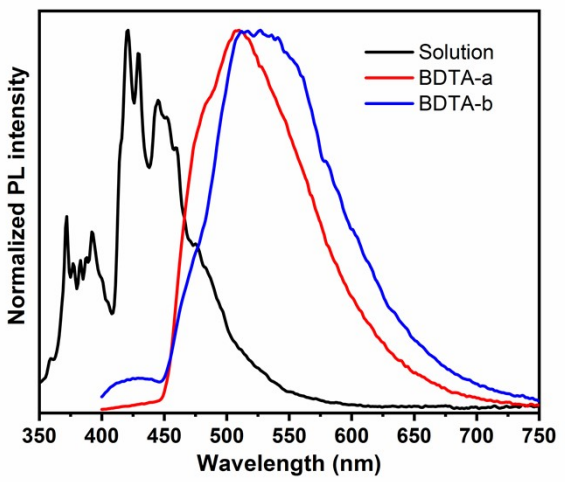

Figure S18. The emission spectra of BDTA in solution and solid states at 77K in air.

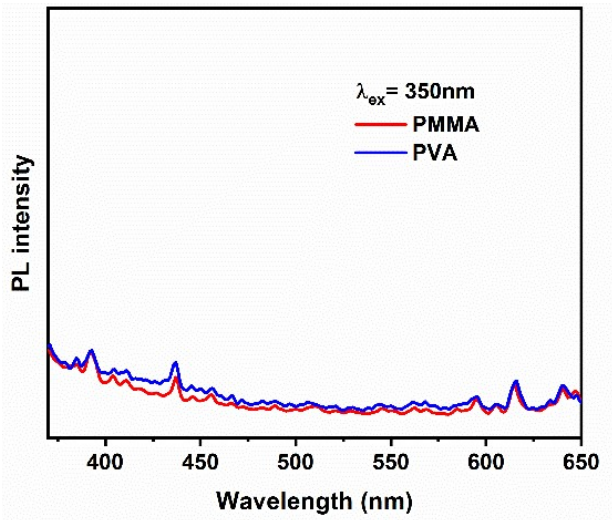

Figure S19. The emission spectra of 0.1 wt% BDTA-doped poly(methyl methacrylate) (PMMA) and poly(vinyl alcohol) (PVA) film.

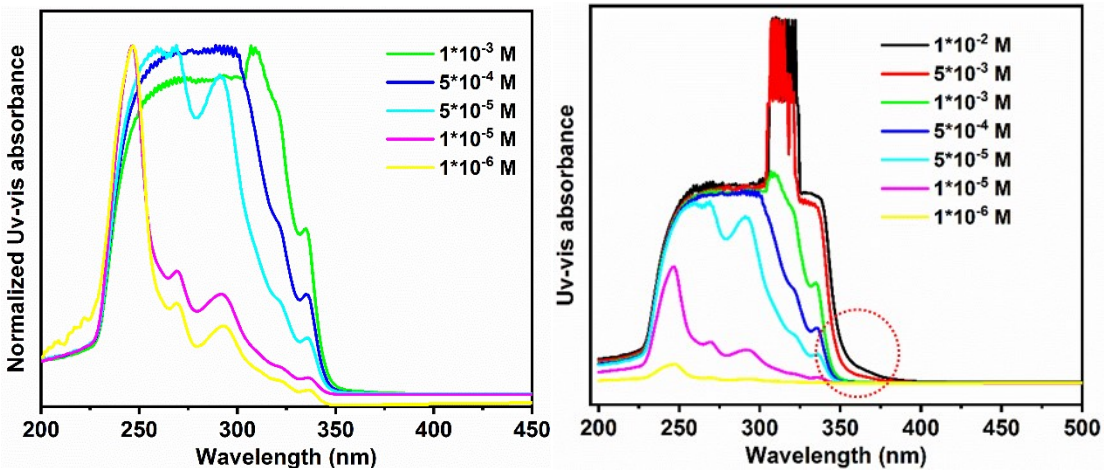

Figure S20. The change of absorption spectrum of BDTA with concentration in 2-methyltetrahydrofuran solution.

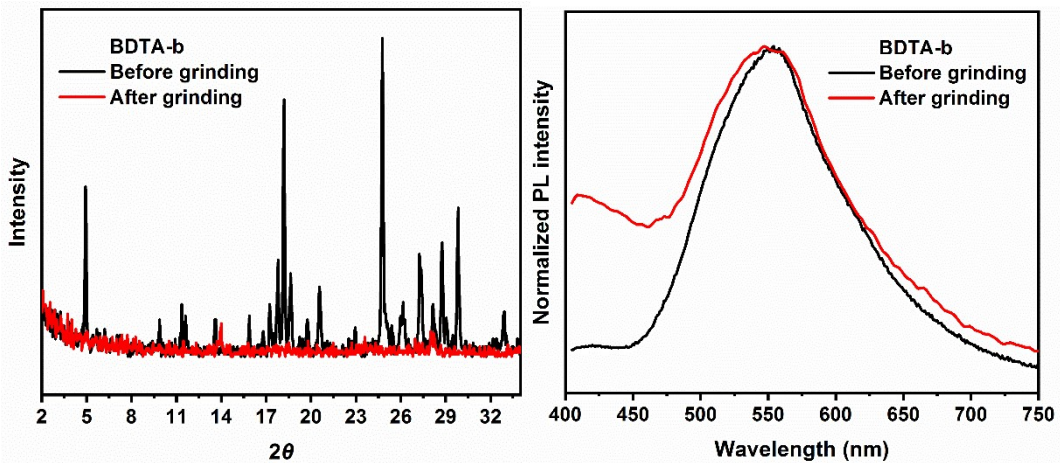

Figure S21. The XRD pattern and the emission spectra of BDTA-b before and after grinding. λ_{ex} = 365 nm.

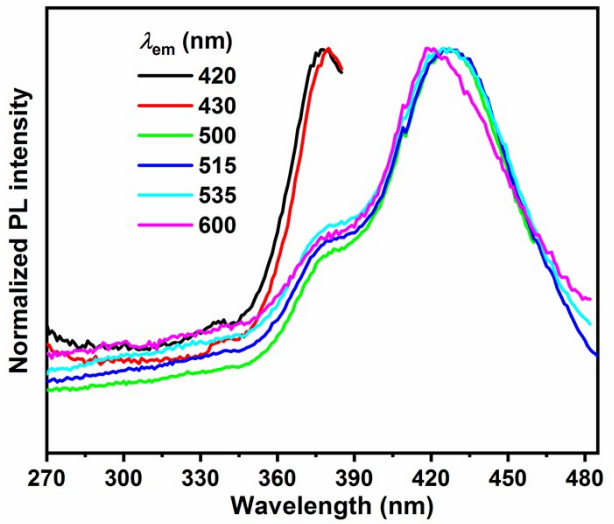

Figure S22. The excitation spectra of BDTA-a monitored at different emission wavelength.

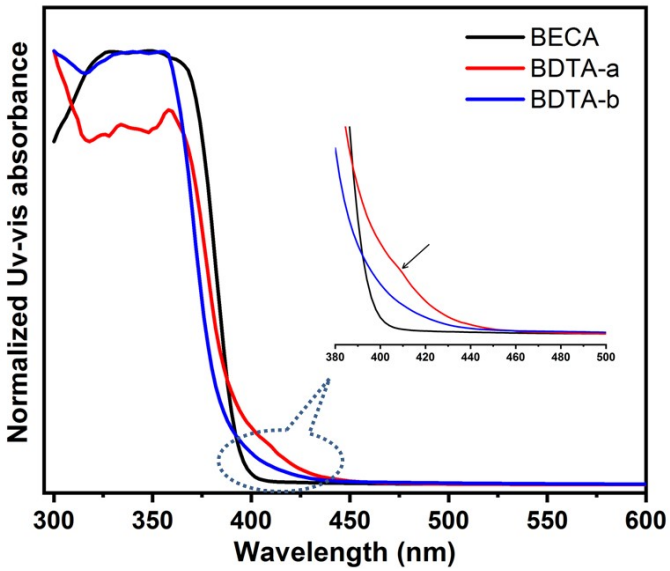

Figure S23. The solid-state absorption spectra.

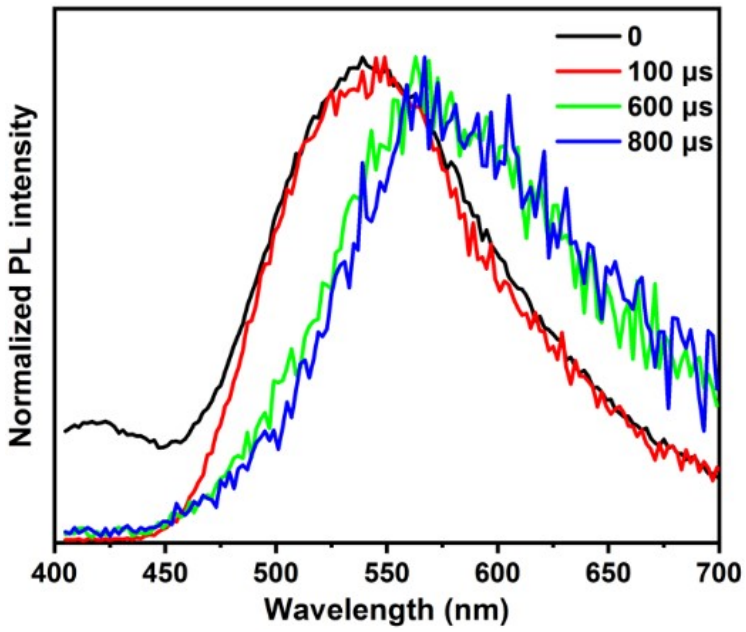

Figure S24. The emission spectrum change of BDTA-a with delay time. λ_{ex} = 375 nm.

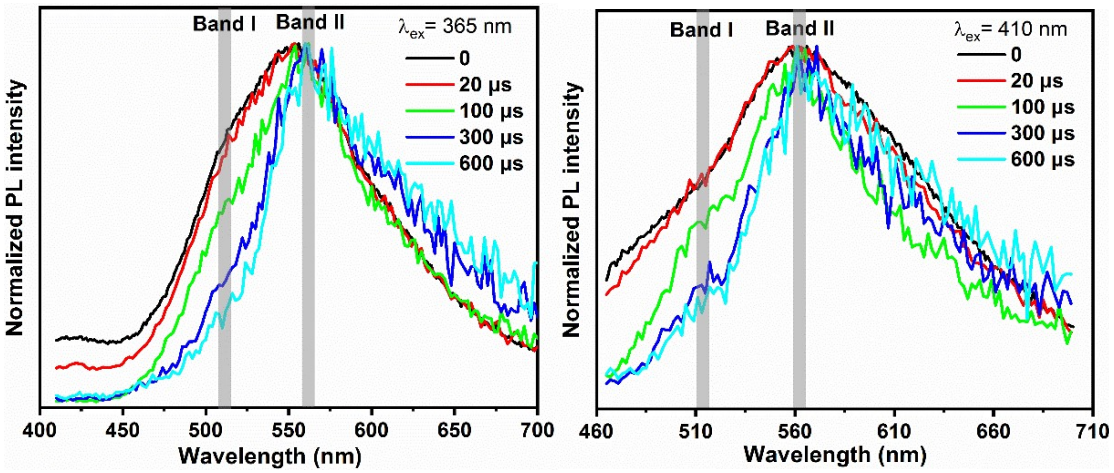

Figure S25. The emission spectrum change of BDTA-b with delay time upon 365 and 410 nm excitation.

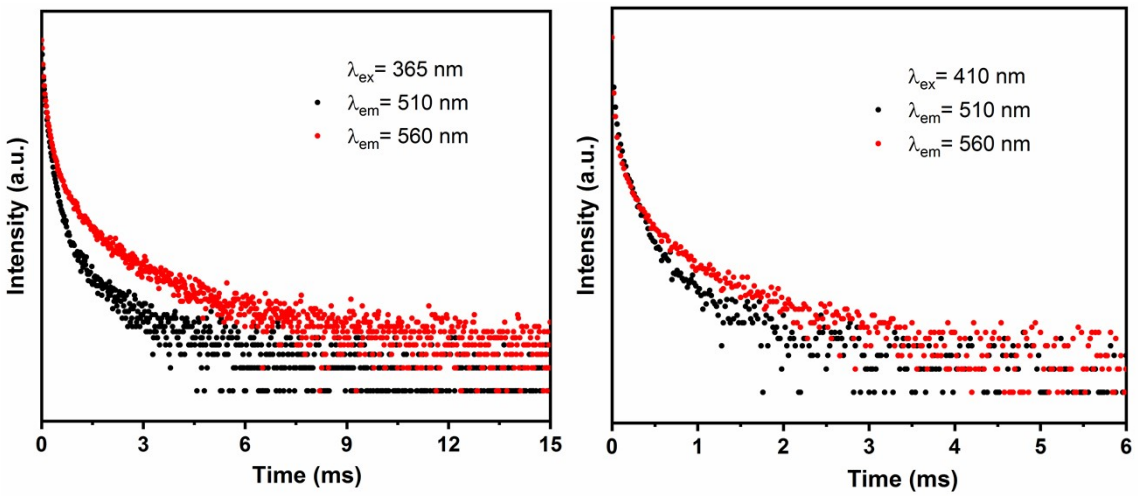

Figure S26. The phosphorescence decay curves of BDTA-b monitored at 510 and 560 nm upon 365 and 410 nm excitation, respectively.

Table S2. The phosphorescence lifetimes of BDTA-b.

λ_{ex} (nm)	λ_{em} (nm)	τ(ms)
365	510	0.17 (57%), 1.00 (43%)
365	560	0.39 (46%), 1.89 (54%)
410	510	0.087 (64%), 0.35 (36%)
410	560	0.089 (50%), 0.56 (50%)

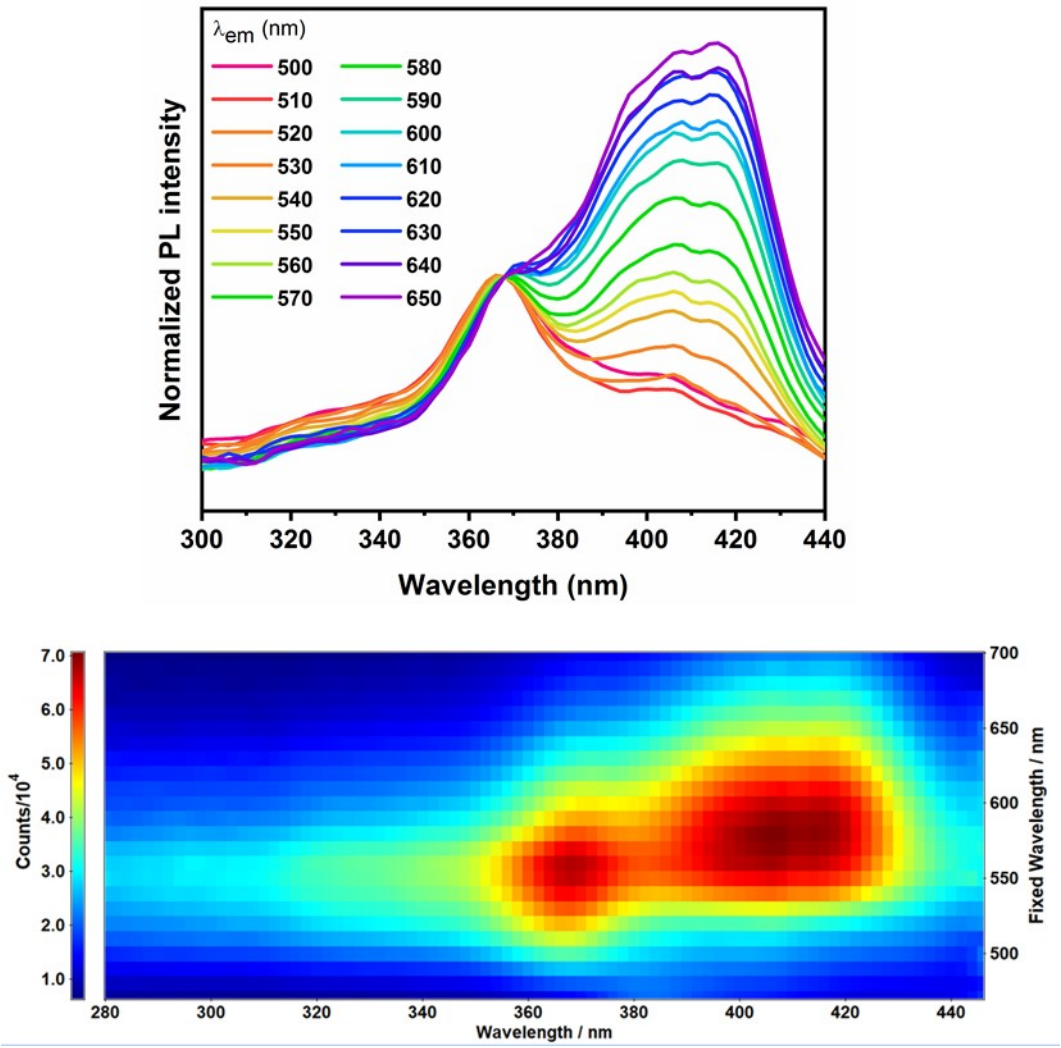

Figure S27. The excitation spectra and map of BDTA-b monitored at different phosphorescence emission wavelength at room temperature.

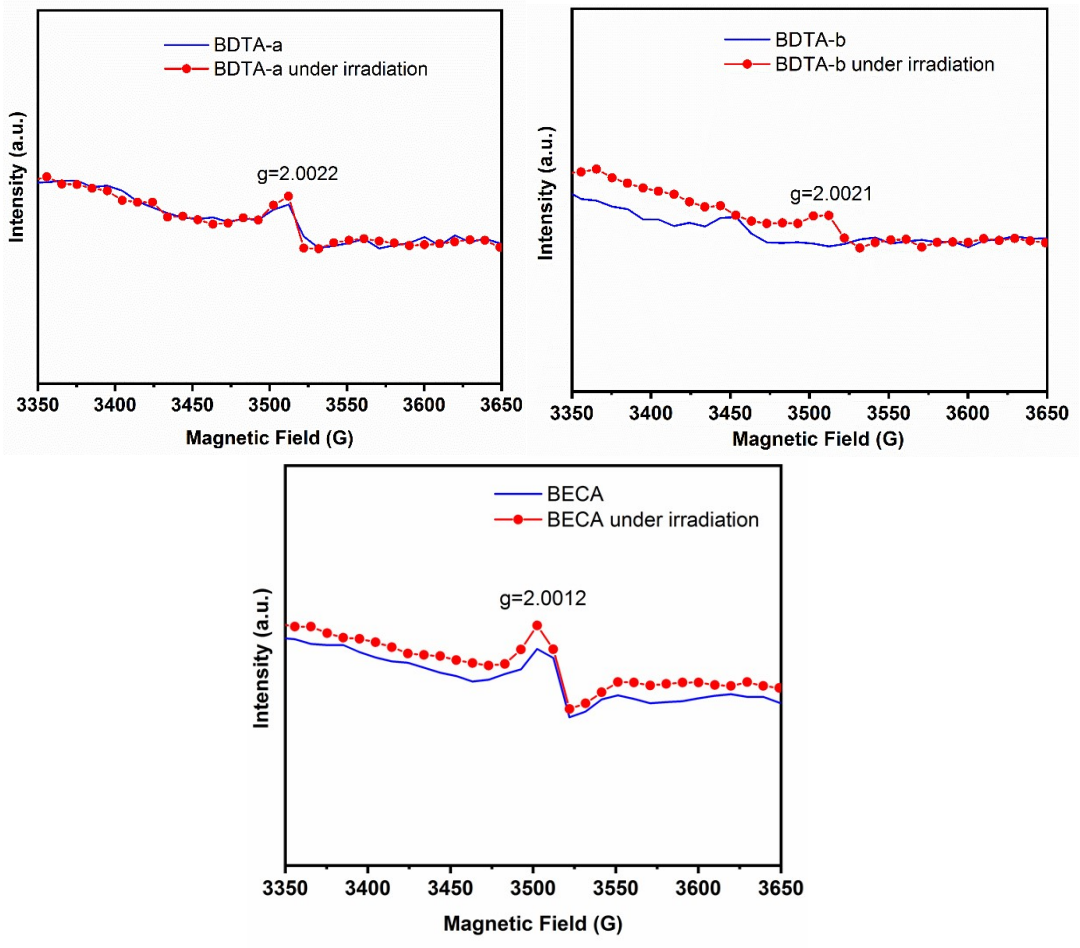

Figure S28. EPR spectra with and without irradiation using a Xe lamp.

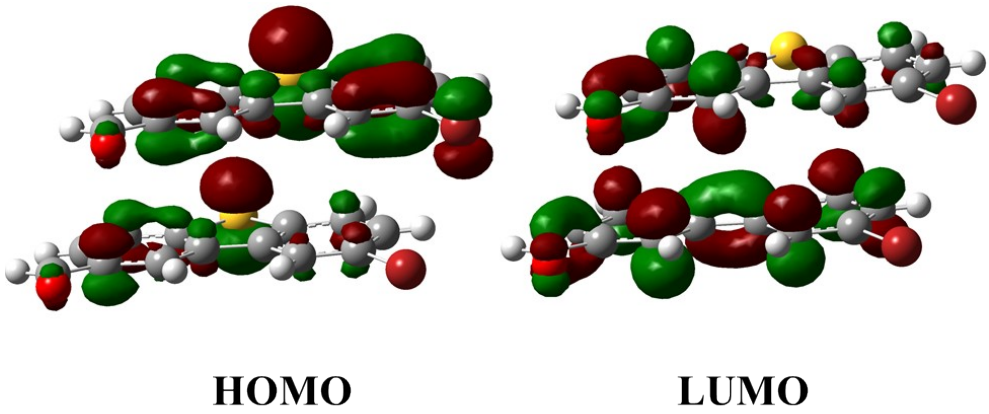

Figure S29. The HOMO and LUMO orbitals of BDTA-a dimer extracted directly from the crystal structure. The orbitals are calculated at CAM-B3LYP/def2-TZVP level. The isovalue is 0.035.

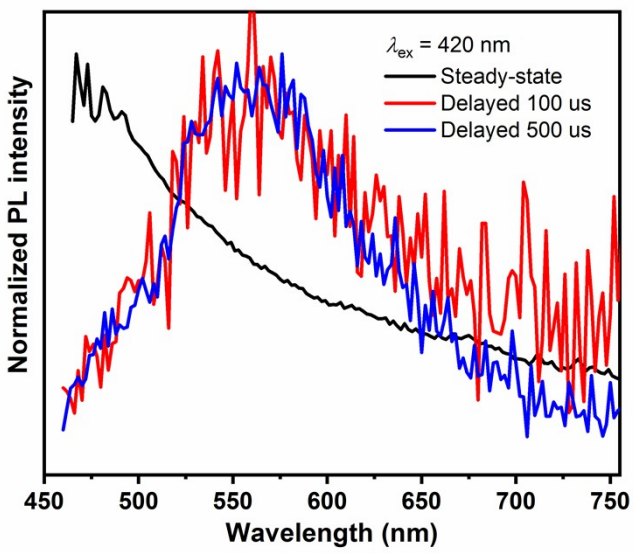

Figure S30. The steady-state and delayed emission spectra of BECA solid at room temperature (λ_{ex} = 420 nm).

Table S3. The calculated SOC-corrected singlet and triplet excited state transition data of BDTA-a dimer extracted from the crystal structure.

T_n	Energy	Transition Character	S_n	Energy	Transition Character	f
T_1	2.977 eV 416.5 nm	π-π*	S_1	4.195 eV 295.6 nm	n-π*	2.5×10^{-4}
T_2	2.990 eV 414.7 nm	π-π*	S_2	4.205 eV 294.9 nm	n-π*	1.6×10^{-4}
T_9	4.023 eV 308.2 nm	π-π*	S_3	4.258 eV 291.2 nm	π-π*	8.3×10^{-4}
T_{10}	4.040 eV 306.9 nm	π-π*	S_4	4.291 eV 289.0 nm	π-π*	1.1×10^{-2}
T_{11}	4.260 eV 291.1 nm	π-π*	S_5	4.640 eV 267.3 nm	π-π*	9.8×10^{-3}
T_{12}	4.266 eV 290.7 nm	π-π*	S_6	4.688 eV 264.5 nm	π-π*	3.2×10^{-3}
T_{16}	4.692 eV 264.3 nm	π-π*				
T_{17}	4.744 eV 261.4 nm	n-π*				
T_{18}	4.776 eV 259.6 nm	n-π*				
T_{19}	4.909 eV 252.6 nm	π-π*				

Table S4. The spin−orbit coupling (SOC) constants (cm^{-1}) of BDTA-a dimer extracted from the crystal structure.

	T_9	T_{10}	T_{11}	T_{12}	T_{13}	T_{14}	T_{15}	T_{16}	T_{17}	T_{18}	T_{19}
S_1	3.94	2.75	2.06	1.56	0.31	1.98	0.46	0.55	0.83	0.29	1.32
S_2	2.52	3.61	2.08	1.95	1.50	0.31	0.70	0.37	0.19	0.17	0.53
S_5	0.50	1.46	0.58	0.34	0.88	0.42	0.85	3.20	16.00	3.73	1.95

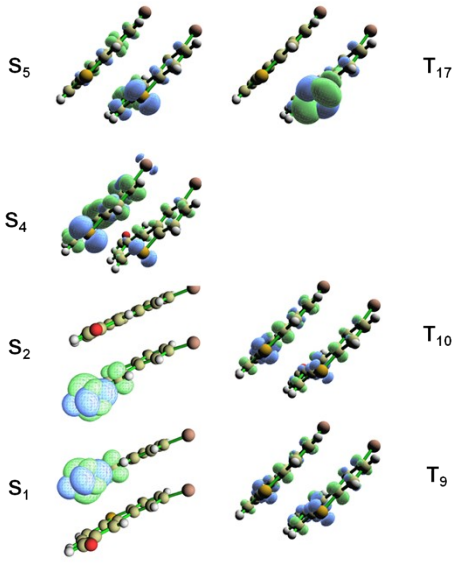

Figure S31. The hole-electron distribution of BDTA-a dimer upon excitation. Green and blue represents electron and hole distributions, respectively. The isosurface value is 0.003.

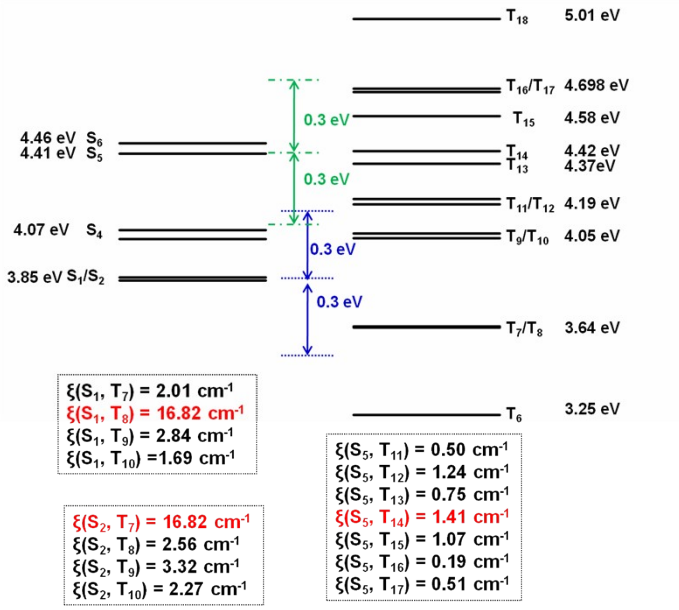

Figure S32. The calculated energy level of BECA dimer and the SOC values (ξ) between interested S and T.

Table S5. The calculated SOC-corrected singlet and triplet excited state transition data of BECA dimer extracted from the crystal structure.

T_n	Energy	Transition Character	S_n	Energy	Transition Character	f
T_1	2.894 eV 428.5 nm	π-π*	S_1	3.846 eV 322.4 nm	n-π*	1.0×10^{-5}
T_2	2.900 eV 427.5 nm	π-π*	S_2	3.860 eV 321.2 nm	n-π*	4.4×10^{-4}
T_7	3.638 eV 340.8 nm	π-π*	S_3	4.031 eV 307.6 nm	π-π*	1.6×10^{-3}
T_8	3.642 eV 340.5 nm	π-π*	S_4	4.071 eV 304.6 nm	π-π*	1.9×10^{-2}
T_9	4.035 eV 307.3 nm	π-π*	S_5	4.410 eV 281.2 nm	π-π*	2.2×10^{-3}
T_{10}	4.056 eV 305.7 nm	π-π*	S_6	4.456 eV 278.3 nm	π-π*	8.2×10^{-4}
T_{11}	4.185 eV 296.3 nm	π-π*				
T_{12}	4.209 eV 294.6 nm	π-π*				
T_{13}	4.366 eV 284.0 nm	π-π*				
T_{14}	4.422 eV 280.4 nm	π-π*				
T_{15}	4.577 eV 270.9 nm	π-π*				
T_{16}	4.684 eV 264.7 nm	π-π*				
T_{17}	4.699 eV 263.9 nm	π-π*				

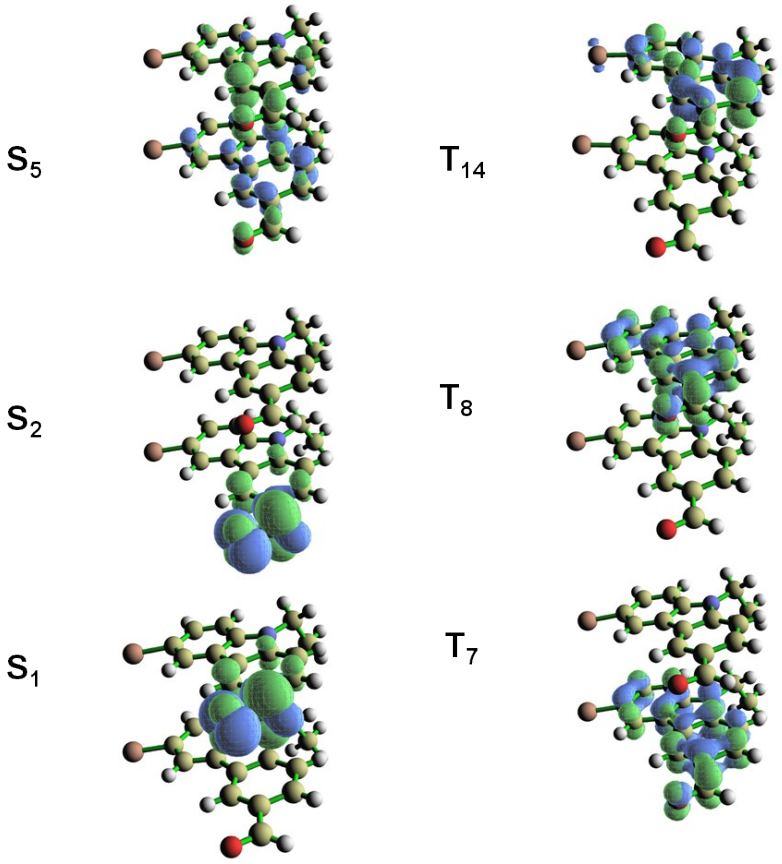

Figure S33. The hole-electron distribution of BECA dimer upon excitation. Green and blue represents electron and hole distributions, respectively. The isosurface value is 0.003.

References

[1] G. M. Sheldrick, *Acta Cryst. A*, **2008**, *64*, 112-122.

[2] O. V. Dolomanov, L. J. Bourhis, R. J. Gildea, J. A. K. Howard, and H. Puschmann, *J. Appl. Cryst.*, **2009**, *42*, 339-341.

[3] M. J. Frisch, G. W. Trucks, H. B. Schlegel, G. E. Scuseria, M. A. Robb, J. R. Cheeseman, G. Scalmani, V. Barone, B. Mennucci, G. A. Petersson, H. Nakatsuji, M. Caricato, X. Li, H. P. Hratchian, A. F. Izmaylov, J. Bloino, G. Zheng, J. L. Sonnenberg, M. Hada, M. Ehara, K. Toyota, R. Fukuda, J. Hasegawa, M. Ishida, T. Nakajima, Y. Honda, O. Kitao, H. Nakai, T. Vreven, J. A. Montgomery, Jr., J. E. Peralta, F. Ogliaro, M. Bearpark, J. J. Heyd, E. Brothers, K. N. Kudin, V. N. Staroverov, T. Keith, R. Kobayashi, J. Normand, K. Raghavachari, A. Rendell, J. C. Burant, S. S. Iyengar, J. Tomasi, M. Cossi, N. Rega, J. M. Millam, M. Klene, J. E. Knox, J. B. Cross, V. Bakken, C. Adamo, J. Jaramillo, R. Gomperts, R. E. Stratmann, O. Yazyev, A. J.

Austin, R. Cammi, C. Pomelli, J. W. Ochterski, R. L. Martin, K. Morokuma, V. G. Zakrzewski, G. A. Voth, P. Salvador, J. J. Dannenberg, S. Dapprich, A. D. Daniels, O. Farkas, J. B. Foresman, J. V. Ortiz, J. Cioslowski, and D. J. Fox, *Gaussian 09*, Revision A.02; Gaussian, Inc.: Wallingford, CT, 2009.

[4] T. Lu, F. Chen, *J. Comput. Chem.*, **2012**, *33*, 580.

[5] Z. Liu, T. Lu, Q. Chen, *Carbon*, **2020**, *165*, 461.

[6] F. Neese, F. Wennmohs, U. Becker, C. Riplinger, *J. Chem. Phys.*, **2020**, *152*, 224108.